Ab Initio Study of Magnetic Tunnel Junctions Based on Half-Metallic and Spin-Gapless Semiconducting Heusler Compounds: Reconfigurable Diode and Inverse Tunnel-Magnetoresistance Effect

T. Aull⦿,* E. Şaşıoğlu⦿, N.F. Hinsche⦿, and I. Mertig⦿

Institute of Physics, Martin Luther University Halle-Wittenberg, Halle (Saale) D-06120, Germany

Magnetic tunnel junctions (MTJs) have attracted strong research interest within the last decades due to their potential use as nonvolatile memory such as magnetoresistive random access memory as well as for magnetic logic applications. Half-metallic magnets (HMMs) have been suggested as ideal electrode materials for MTJs to achieve an extremely large tunnel-magnetoresistance (TMR) effect. Despite their high TMR ratios, MTJs based on HMMs do not exhibit current rectification, i.e., a diode effect, which was achieved in a magnetic tunnel junction concept [E. Şaşıoğlu *et al.*, ACS Appl. Electron. Mater. 1, 1552–9 (2019)] based on HMMs and type-II spin-gapless semiconductors (SGSs). The proposed concept has recently been experimentally demonstrated using Heusler compounds. In the present work, we investigate from first-principles MTJs based on type-II SGS and HMM quaternary Heusler compounds FeVTaAl, FeVTiSi, MnVTiAl, and CoVTiSb. Our *ab initio* quantum transport calculations based on a nonequilibrium Green's function method have demonstrated that the MTJs under consideration exhibit current rectification with relatively high on:off ratios. We show that, in contrast to conventional semiconductor diodes, the rectification bias voltage window (or breakdown voltage) of the MTJs is limited by the spin gap of the HMM and SGS Heusler compounds. A unique feature of the present MTJs is that the diode effect can be configured dynamically, i.e., depending on the relative orientation of the magnetization of the electrodes, the MTJ allows the electrical current to pass either in one or the other direction, which leads to an inverse TMR effect. The combination of nonvolatility, reconfigurable diode functionality, tunable rectification voltage window, and high Curie temperature of the electrode materials makes the proposed MTJs very promising for room-temperature spintronic applications and opens ways to magnetic memory and logic concepts as well as logic-in-memory computing.

I. INTRODUCTION

The current computing technology is based on the von Neumann architecture [1], in which the central processing unit and the memory are connected via a shared bus system, causing the memory bandwidth bottleneck and high power consumption. It was demonstrated that, for many computing tasks, the majority of the energy and time is needed to transfer data between the memory and the CPU, rather than the information processing itself [2,3]. To tackle the bandwidth bottleneck in today's microprocessors, information processing concepts such as logic-in-memory computing are receiving substantial interest [4–9]. The logic-in-memory computing architecture requires nonvolatile memory elements. Among the emerging nonvolatile memory technologies, the magnetoresistive random access memory (MRAM) is the most promising candidate due to its almost infinite endurance. The MRAM combines relatively high access speeds with nonvolatility. In particular, spin-transfer torque (STT) MRAM and spin-orbit torque (SOT) MRAM emerged as promising candidates to replace the L3 and L2 caches [10,11] of modern microprocessors.

In conventional magnetic tunnel junctions (MTJs), a nonmagnetic insulator of a few nanometer thickness is sandwiched between two ferromagnetic electrodes [12,13]. Thus, the electronic transport is spin dependent and mainly determined by quantum tunneling. For this reason, the tunnel-magnetoresistance (TMR) ratio and the conductance are very important quantities of MTJs [14–17]. The resistance of such devices differs in two configurations, when the magnetization of the left and right electrodes is parallel oriented and when the orientation is switched to antiparallel, resulting in the TMR effect. When no bias voltage is applied, the TMR ratio is defined as TMR $= (G_{\uparrow\uparrow} - G_{\uparrow\downarrow})/(G_{\uparrow\downarrow} + G_{\uparrow\uparrow})$, where $G_{\uparrow\uparrow}$ ($G_{\uparrow\downarrow}$) denotes the conductance in the parallel (antiparallel) configuration of the electrodes. For finite biases, the TMR expression

---

*thorsten.aull@physik.uni-halle.de

becomes TMR $= (I_{\uparrow\uparrow} - I_{\uparrow\downarrow})/(I_{\uparrow\downarrow} + I_{\uparrow\uparrow})$, where $I_{\uparrow\uparrow}$ $(I_{\uparrow\downarrow})$ is the tunnel current through the device in the parallel (antiparallel) orientation of the magnetization of the electrodes. It is worth noting that the tunnel barrier material, as well as the thickness of the tunnel barrier, and the applied bias voltage can influence the TMR effect [13,18,19]. Another factor that can affect the sign and the value of the TMR ratio is a structural asymmetry in the junctions. Heiliger *et al.* [20,21] proposed that, independent of the applied bias voltage, in asymmetric junctions the value of $I_{\uparrow\downarrow}$ exceeds the value of $I_{\uparrow\uparrow}$ and, as a consequence, leads to a negative TMR ratio. The dependency of the TMR ratio on the applied bias voltage for both the normal and the inverse TMR effect is schematically illustrated in Fig. 1(a).

MTJs played a significant role in spintronics development as they are suitable for several applications ranging from read-head sensors to nonvolatile memory devices such as STT MRAM and SOT MRAM and from nonvolatile logic concepts to logic-in-memory computing [22–24]. Magnetic logic promises nonvolatile, low-power computing and up to now, several different approaches have been proposed such as the quantum cellular automata [25,26], domain-wall logic [27,28], MTJ logic [29–31], etc. The latter is of particular interest because it opens the way to logic-in-memory computing, i.e., storing and processing the data within the same chip and thus providing an opportunity to explore computing architectures beyond the classical von Neumann architecture [32,33]. MTJ-based magnetic logic proposals can be divided into three categories: (i) external field-driven MTJ logic, (ii) spin Hall effect driven MTJ logic, and (iii) logic based on magnetic tunnel diodes and magnetic tunnel transistors.
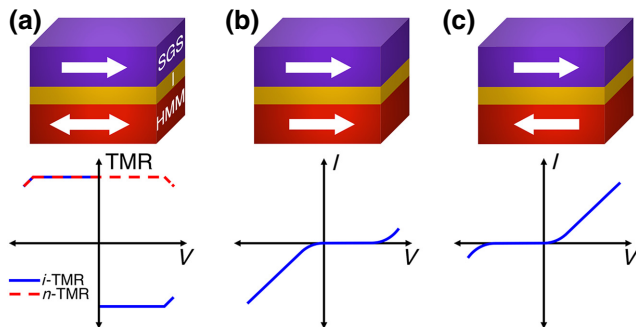

FIG. 1. (a) Top: schematic representation of the magnetic tunnel junction based on a half-metallic magnet and a spin-gapless semiconductor. Bottom: dependency of the TMR effect on the bias voltage in MTJs. The inverse (i-)TMR effect is illustrated by a blue line while the normal (n-)TMR effect is represented by a red dashed line. (b),(c) The same as (a) for the parallel and antiparallel orientations of the magnetization directions of the electrodes as well as the corresponding current-voltage (*I-V*) characteristics. The white arrows indicate the magnetization direction of the electrodes.

In the first category, the logic gates are built from MTJs, which are arranged in a bridge-type configuration and the logic inputs are provided by external wires, which creates a magnetic field that switches the magnetization direction of one electrode in the MTJ. In this way, all logic gates can be realized with few MTJs [29,30,34]. The utilization of an inverse TMR effect can even further reduce the number of MTJs in logic gates [31,35]. However, the drawback of this approach is that it is not scalable due to input wires and their routing near the MTJs. In the second category, the logic gates are based on a four-terminal spin Hall effect driven MTJ with fully electrically separated write and read paths [36–38]. These four-terminal MTJ devices can overcome the challenges of operation gain and direct cascading in current spintronic logic circuits. Moreover, simulations have indicated that correct logic fan-out operation can be achieved with a voltage below 150 mV, which is promising for low-power computing [38]. Note that in both approaches the logic operation gain (i.e., output voltage margin) depends mainly on the TMR ratio of the MTJs. While in the third category, a MTJ possesses, in addition to the TMR effect (memory), a current rectification (diode effect) functionality. Such MTJs also constitute the basic building blocks of the three-terminal magnetic tunnel transistors for logic applications. The TMR effect and current rectification have been observed for single barrier asymmetric MTJs as well as for double barrier MTJs with tunnel barriers of different transparencies [39–42]. Although in initial studies of magnetic tunnel transistors low magnetocurrent ratios and transfer rates α are reported [43–47], in recent experiments of fully epitaxial magnetic tunnel transistors a large magnetocurrent ratio and transfer rate α is detected [48]. Besides being the basic building blocks of the three-terminal magnetic tunnel transistors, the MTJ possessing the diode effect is of particular interest for high-density three-dimensional (3D) cross-point STT-MRAM applications as it eliminates the need for an additional selection device [42], i.e., a MOSFET transistor or a *p-n* diode [49–51].

In contrast to MTJ-based logic proposals, in the first and second categories as well as other concepts like spin-orbit torque logic [52] not mentioned above (for a detailed discussion, we refer the reader to Refs. [53,54], which report a benchmarking of beyond-CMOS devices including various spintronic logic concepts), magnetic tunnel diodes and transistors can operate extremely high frequencies, i.e., in the terahertz regime, making them ideal candidates for high-speed electronic and spintronic applications. However, despite terahertz operation frequencies, conventional magnetic tunnel diodes and transistors come with fundamental issues such as low on:off current ratios and less asymmetric current-voltage characteristics in diodes and base-collector leakage currents in transistors, which might lead to high power dissipation. In Ref. [55], we proposed a magnetic tunnel diode and transistor concept, which

overcomes the limitations of conventional magnetic tunnel devices and provides additional unique functionalities like reconfigurability, which was recently experimentally demonstrated [56]. The concept is based on spin-gapless semiconductors (SGSs) [57] and half-metallic magnets (HMMs) [58]. The two-terminal magnetic tunnel diode (or MTJ) is comprised of a SGS electrode and a HMM electrode separated by a thin insulating tunnel barrier. A schematic representation of the structure of the reconfigurable magnetic tunnel diode is shown in Figs. 1(b) and 1(c). Depending on the relative orientation of the magnetization of the electrodes, the MTJ allows the electrical current to pass either in one or the other direction.

The aim of the present paper is a computational design of MTJs based on HMM and SGS quaternary Heusler compounds for room-temperature device applications. Heusler compounds offer a unique platform to realize MTJs as these materials possess very high Curie temperatures (above room temperature) as well as HMM and SGS behavior within the same family [59–61]. To this end, the selection of the HMM and SGS electrode materials from the quaternary Heusler family for the design of MTJs is based on our recent study in Ref. [61]. We stick to SGS FeVTaAl and FeVTiSi compounds due to their large energy gaps in opposite spin channels around the Fermi level [61], MgO as the tunnel barrier due to the lattice matching, and for the HMMs, although we have a large variety of choice, we choose MnVTaAl and CoFeVSb since both materials exhibit nearly symmetric spin gaps above and below E_F and possess similar lattice constants to MgO. *Ab initio* quantum transport calculations based on the nonequilibrium Green's function (NEGF) method have demonstrated that the MTJs based on HMM and SGS Heusler compounds exhibit, in addition to the inverse TMR effect, current rectification, i.e, diode effect, which can be dynamically configured. We show that in contrast to semiconductor diodes (*p-n* diode or Schottky diode), the rectification voltage window (or breakdown voltage) of these MTJs is limited by the spin gap of HMM and SGS Heusler compounds. The calculated zero temperature on:off current ratios vary between 10^2–10^7, being lowest for the FeVTiSi/MgO/CoFeVSb MTJ, which can be attributed to the overlap of the conduction and valence bands of opposite spin channels around the Fermi level. The combination of nonvolatility and the dynamically reconfigurable diode effect as well as the very high Curie temperature of quaternary Heusler compounds makes the proposed MTJs very promising for room-temperature spintronic memory and logic applications. The rest of the paper is organized as follows. In Sec. II, we discuss the *I-V* characteristics of the MTJ concept by using the spin-dependent energy-band diagrams. In Sec. III, we present the computational details of our study. Our computational results are presented and discussed in Sec. IV, and finally, in Sec. V, we give our summary and outlook.
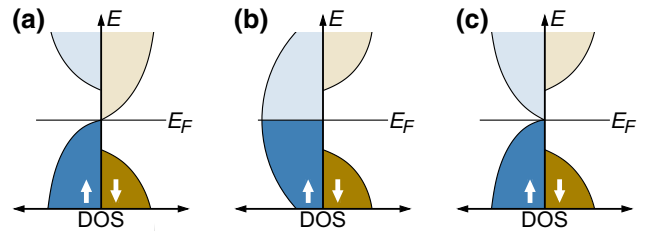

FIG. 2. Schematic representation of the density of states for a (a) type-II spin-gapless semiconductor, (b) half-metallic magnet, and (c) type-I spin-gapless semiconductor.

II. HMM/I/SGS MAGNETIC TUNNEL JUNCTIONS

In Figs. 1(b) and 1(c), we schematically show a MTJ based on a HMM and a SGS in the parallel and antiparallel configurations of the electrodes, respectively, together with the corresponding *I-V* curves. HMMs have been used as electrode materials for MTJs to achieve extremely large TMR effects. Despite their large TMR ratios, the MTJs based on HMMs do not present current rectification, i.e., a diode effect. In Ref. [55], it was proposed that replacing one of the HMM electrodes with a SGS material in a MTJ gives rise to additional functionalities, i.e., current rectification, inverse TMR effect, and reconfigurability of the MTJ. Such a MTJ is also called a reconfigurable magnetic tunnel diode [55]. Besides the HMM, the SGS material is the key component of this MTJ. SGSs have been proposed by Wang in 2008 as a theoretical concept [57]. By employing first-principles calculations, Wang demonstrated that doping $PbPdO_2$ with Co atoms results in a new class of materials: the SGSs [57,62]. Since then, different classes of materials have been predicted to present SGS behavior of various types, i.e., from type-I to type-IV SGSs [57,59–61,63–65] and some of the predicted SGSs have been experimentally realized [66]. Since type-II SGSs are the key component of the reconfigurable MTJ, in Fig. 2 we present the schematic density of states (DOS) of a type-II SGS together with a conventional HMM as well as a type-I SGS, which can also be used as a replacement of the HMM in a MTJ. As seen in Fig. 2(a), the type-II SGS possesses a unique electronic band structure, i.e., it presents a finite gap below and above the Fermi level E_F in different spin channels, while the valence and conduction bands of different spin channels touch at E_F. On the other hand, in HMMs, the majority-spin channel behaves like in normal metals, but the minority-spin channel exhibits a gap around the Fermi level like in a semiconductor or insulator. The DOS of type-I SGSs is similar to HMMs [see Figs. 2(b) and 2(c)]. The minority-spin channel looks the same, while in the majority-spin channel a zero-width gap appears at the Fermi level since the conduction- and valence-band edges touch at E_F.

The operation principle of the reconfigurable MTJ is extensively discussed in Ref. [55] and hence here we
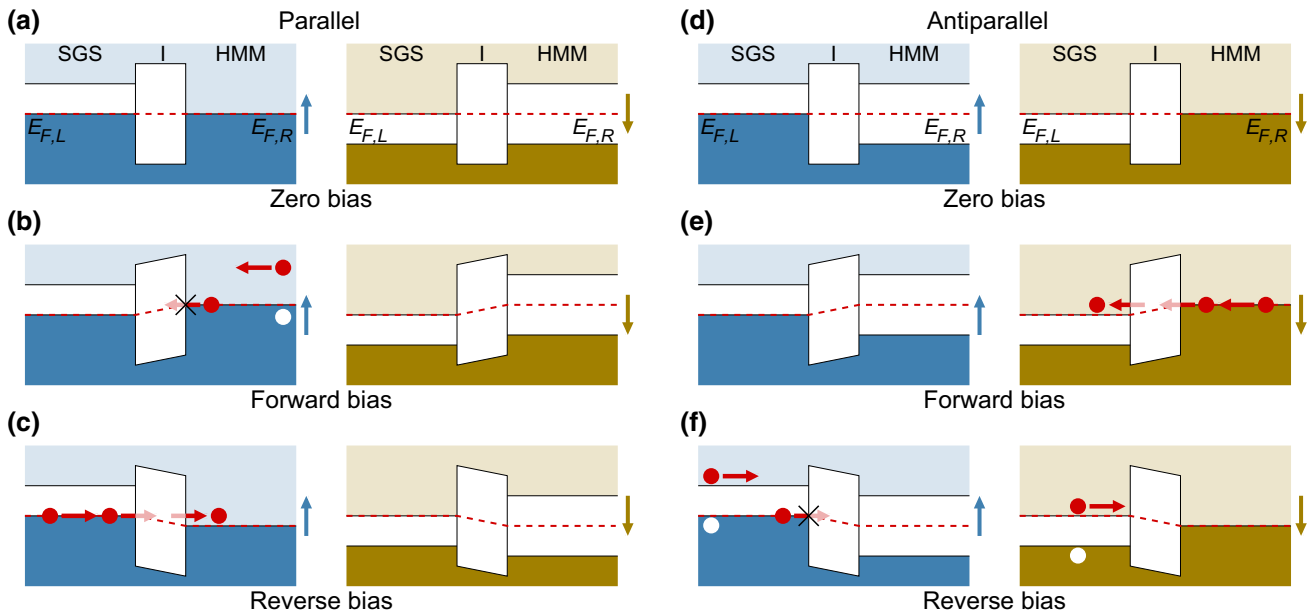
FIG. 3. Schematic representation of the spin-resolved energy-band diagram for the SGS/I/HMM MTJ for parallel (P) orientation of the magnetization directions of the electrodes (a) for zero bias, (b) under forward bias, and (c) under reverse bias. The electrons (holes) and the Fermi energy are denoted by red (white) spheres and a dashed line, respectively, and the tunneling process is illustrated by partly shaded red arrows. Panels (d)–(f) represent the same as (a)–(c) for the antiparallel (AP) orientation of the magnetization directions of the electrodes [see Figs. 1(b) and 1(c)].

present a short overview of the concept by using the spin-resolved energy-band diagram shown in Fig. 3. The spin-resolved energy-band diagram is based on the schematic densities of states provided in Figs. 2(a) and 2(b), i.e., the type-II SGS material possesses a gap in the minority-spin (majority-spin) channel below (above) the Fermi level while the HMM exhibits a gap in the minority-spin channel around the Fermi energy. We further assume that the type-II SGS electrode, the tunnel barrier, and the half-metallic material have the same work function and equal Fermi levels and therefore we do not consider charge transfer at the interfaces. However, real materials, as will be discussed in Sec. IV, possess different work functions and so there occurs charge transfer between one material and the other at the interface, which might cause a band bending in the SGS electrode. Moreover, due to interactions at the interface, the junction materials might not conserve the SGS or HMM characteristics close to the interface and thus the band diagram will not be as sharp as presented in Fig. 3.

The I-V characteristics of the SGS/I/HMM junction illustrated in Figs. 1(b) and 1(c) can be qualitatively explained by Bardeen's approach for tunneling [67,68]. For a simple tunnel barrier, the tunnel current $I(V)$ is given by the expression

$$I(V) \sim \sum_\sigma \int_{-\infty}^{+\infty} \rho_{\text{HMM}}^\sigma(E + eV)\rho_{\text{SGS}}^\sigma(E)|T(V)|^2$$
$$\times [f(E) - f(E + eV)]dE,$$

where $\rho_{\text{SGS}}^\sigma(E)$ and $\rho_{\text{HMM}}^\sigma(E + eV)$ denote the densities of states of the SGS and HMM electrodes with spin σ, $f(E)$ is the Fermi distribution function, and $T(V)$ is the transmission probability, which is proportional to $e^{-d\sqrt{\phi - \bar{V}}}$, where d is the thickness of the tunnel barrier and ϕ is the barrier height. As shown in Fig. 3(b), when the magnetization directions of the electrodes are aligned parallel and a positive bias voltage (forward bias) is applied to the SGS electrode, electrons in the occupied majority-spin valence band of the HMM electrode cannot tunnel through the insulating barrier into the SGS electrode because there are no available states above the Fermi energy in the majority-spin channel of the SGS electrode unless a certain bias voltage is reached. For minority-spin electrons, the HMM electrode behaves like an insulator and thus no electron transport takes place. For a negative bias voltage (reverse bias), electrons in the majority-spin channel in the SGS material can tunnel into the unoccupied states of the HMM, as shown in Fig. 3(c). In the minority-spin channel, neither in the SGS electrode nor in the HMM electrode are states available that can contribute to a current. Thus, the tunneling current through the MTJ is 100% spin polarized. A similar discussion holds for the antiparallel orientation of the magnetization direction of the SGS and HMM electrodes, for which the corresponding energy-band diagram is presented in Figs. 3(d)–3(f). Note that in the schematic representation of the I-V characteristics of the MTJ [see Figs. 1(b) and 1(c)], we use the standard definition of current for semiconductor devices, i.e., the current

direction is opposite to the electron motion direction, while in Ref. [55], the same direction is taken for the current and electron motion. This is why the *I-V* characteristics are different in Ref. [55].

The presence of the reconfigurable diode effect in MTJs based on SGSs and HMMs leads to an inverse TMR effect rather than a normal TMR effect as in most of the conventional MTJs. The voltage dependence of the TMR presented in Fig. 1(a) can be explained on the basis of the *I-V* characteristics discussed above. For a positive (forward) bias voltage, $I_{\uparrow\downarrow}$ will take a finite value while $I_{\uparrow\uparrow}$ is equal to zero. For a negative (reverse) bias voltage, the situation is exactly the opposite. Thus, for forward bias, the TMR ratio will take the value -100% in a bias voltage window, which is set by the band gap of the SGS and HMM electrodes. Similarly, under a reverse bias, the TMR ratio will be normalized to $+100\%$. Note that we use here a different definition of the TMR ratio compared to the Jullière model [69].

Up to now, the discussion of the *I-V* curves and voltage dependence of the TMR effect in SGS/I/HHM MTJs was based on the schematic energy-band diagram at zero temperature and perfect SGS behavior of the electrode material. However, at finite temperatures, thermally excited electrons (non-spin-flip processes) can be transmitted from one electrode to the other in the off state and thus cause a leakage current [see Figs. 3(b) and 3(f)]. This reduces the on:off and TMR ratios. Nevertheless, such processes can be significantly reduced by increasing the band gap of the SGS and HMM materials as the Fermi-Dirac distribution function decays exponentially with increasing energy. Besides thermally excited non-spin-flip electrons, spin-flip processes stemming from spin-orbit coupling and electron-magnon interaction can also reduce the on:off ratio as well as the TMR effect [70–72].

III. COMPUTATIONAL DETAILS

Our *ab initio* study of the SGS/MgO/HMM MTJs is based on spin-polarized density functional theory (DFT) using the QuantumATK software package (version S-2021.06) [73,74]. We use linear combinations of atomic orbitals as the basis set together with norm-conserving PseudoDojo pseudopotentials [75] with the Perdew-Burke-Ernzerhof (PBE) parametrization of the exchange-correlation functional [76]. For the determination of the ground-state properties, we use a $15 \times 15 \times 15$ Monkhorst-Pack **k**-point grid and as density mesh cutoff 145 Hartree. Since the PBE parametrization is well known to underestimate band gaps [77–79], we use the DFT-1/2 method [80,81] as implemented in the QUANTU-MATK package to correct the band gap in the calculations of the transmission spectra. The changes in the SGS and HMM band structure by employing the DFT-1/2 method are negligible. For the structural optimization, all forces

converge to at least 0.01 eV/Å and self-consistency is achieved when the energies between two steps of the SCF cycle differ by less than 10^{-4} eV. For the transport calculations, we employ the NEGF approach combined with the DFT method using an $11 \times 11 \times 115$ **k**-point mesh. For all calculations, the smearing is set to 26 meV. To calculate the *I-V* characteristics, QuantumATK applies the Landauer-Büttiker approach [82], where $I(V) = (e/h)$ $\sum_{\sigma} \int T^{\sigma}(E,V)[f_L(E,V) - f_R(E,V)]dE$, where $f_L(E,V)$ and $f_R(E,V)$ represent the Fermi-Dirac distributions of the left and right electrodes, respectively. Furthermore, the transmission coefficient $T^{\sigma}(E,V)$ depends on the spin σ of the electrons, the applied bias voltage V, and the energy E. For the calculation of $T^{\sigma}(E,V)$, we choose a dense 100×100 **k**-point mesh. Moreover, the self-consistent *I-V* calculations are compared with a zero-bias linear response approach. It is worth noting that, for the linear response approach, the transmission spectrum is treated as bias independent, and thus this approximation is not valid for large biases and therefore just allows for a qualitative description of the *I-V* characteristics.

IV. RESULTS AND DISCUSSION

In Sec. II, we qualitatively discussed the *I-V* characteristics of the MTJs based on SGSs and HMMs using the spin-dependent energy-band diagram and a simple tunnel barrier model. However, quantum tunneling is a very sophisticated process in real materials as it depends on the symmetry of the wave functions in the electrodes, their decay rate, and their matching at the interface. The decay rate is determined by the thickness and barrier height as well as the complex energy bands of the insulating material [83,84]. Therefore, fully *ab initio* quantum transport calculations are needed to determine the *I-V* characteristics of the MTJs based on SGSs and HMMs. We choose FeVTaAl and FeVTiSi quaternary Heusler compounds as SGS electrodes together with MnVTiAl and CoFeVSb as HMM electrodes and construct two different types of MTJs. All four electrode materials possess Curie temperatures above room temperature, as presented in Table I. To construct the MTJs, we take the type-II SGS electrode material in the cubic structure and relax the tunnel barrier MgO as well as the HMM electrode material with respect to the in-plane lattice parameter of the first electrode. For this reason, we include the c/a ratios for the HMM electrodes and MgO, respectively, which take the tetragonal structure in Table I. The atomic structure of one MTJ is illustrated in Fig. 4(a). The left electrode FeVTaAl is a SGS, the right electrode MnVTiAl is a HMM, and MgO acts as a tunnel barrier. The FeVTaAl (MnVTiAl) has two types of interface terminations with MgO: FeV and TaAl (MnV and TiAl). Our total energy calculations have shown that the FeV-MgO (MnV-MgO) termination possesses lower energy. Similarly, as for
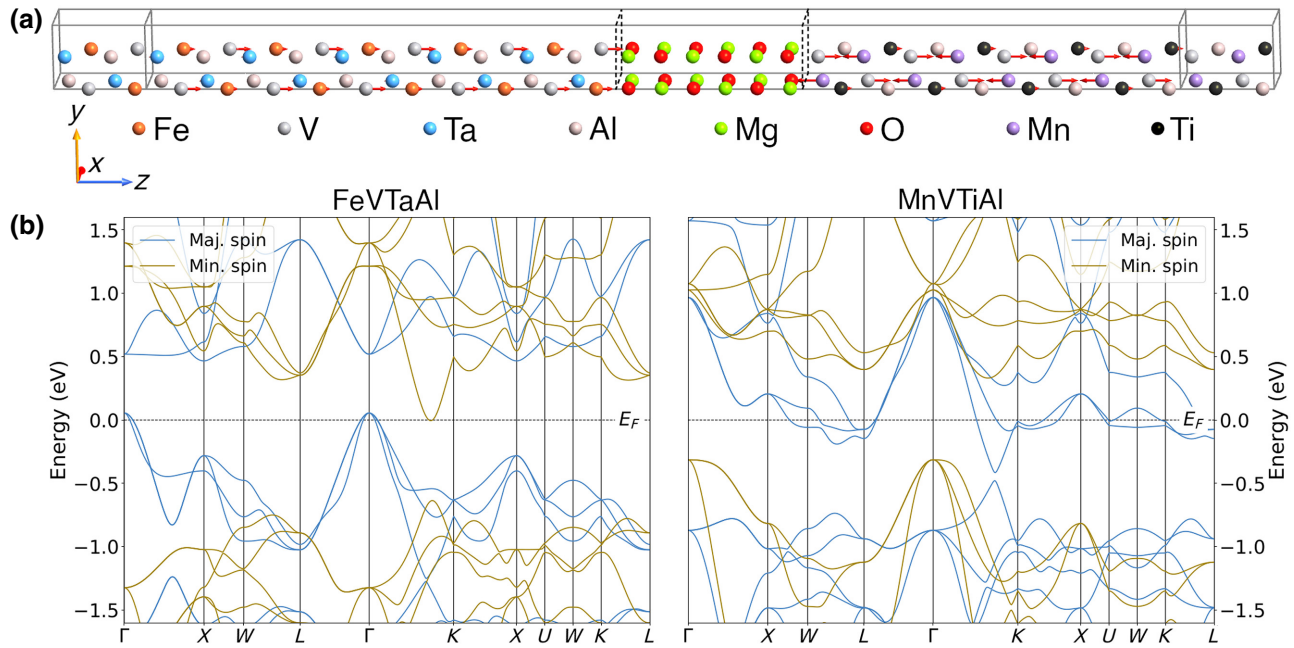
FIG. 4. (a) The atomic structure of the FeVTaAl/MgO/MnVTiAl tunnel junction. The system is periodic in the *x*-*y* plane orthogonal to the *z* axis, which is the transport direction. The red arrows mark the direction and the size of the magnetic moments within the scattering region. The small induced magnetic moments are overlayed by the atomic radii. The black dashed boxes illustrate the interface. (b) The calculated spin-resolved bulk band structures of the fcc unit cell for FeVTaAl (left panel) and MnVTiAl (right panel). The dashed black line denotes the Fermi level that is set to zero.

the second MTJ FeVTiSi/MgO/CoFeVSb (see Table I), the FeV-MgO (CoFe-MgO) termination has lower energy.

For both MTJs, the thickness of the MgO tunnel barrier varies between three and six monolayers (0.6–1.4 nm) and the SGS and HMM electrodes are constructed by repeating the minimal tetragonal unit cell 5 times along the [001] direction. Depending on the number of MgO layers, the length of the device (screening region) lies between 60 and 66 Å. The device is periodic in the *x*-*y* plane and the *z* direction is the transport direction. We adjust the alignment of the magnetic moments to the *z* axis. The direction and magnitude of the atomic magnetic moments of the electrode materials in the MTJ are respectively represented by the red arrows and their size in Fig. 4(a). At both interfaces, the magnetic moments deviate from their bulk values (see Table I). At the FeVTaAl-MgO interface, the largest difference is obtained for the Fe atom whose magnetic moment increases from $0.85\mu_B$ to $1.82\mu_B$, while the moment of the Ta atom changes from about $0.2\mu_B$ to $-0.4\mu_B$. The changes at the remaining atoms are negligible. Similar behavior is observed for the MnVTiAl-MgO interface, where the largest deviation occurs in the magnetic moment of the Mn atom, whose value increases from $-2.42\mu_B$ to $-3.30\mu_B$, while the magnetic moments of the other atoms remain more or less unchanged.

Next, we discuss the electronic properties of the FeVTaAl/MgO/MnVTiAl junction at zero bias, i.e., in equilibrium. Thus, we present the bulk band structures

of both junction materials in Fig. 4(b). The MnVTiAl compound exhibits a nearly symmetric band gap of 330 meV above and 310 meV below the Fermi level in the minority-spin channel, while FeVTaAl exhibits a type-II SGS behavior. As discussed above, the strong variation of the magnetic moments at the interface implies that the HMM and SGS properties are also lost. The loss of the HMM and SGS properties stems from two factors: (i) the electronic structure, i.e., the Fe and V (Mn and V) atoms at the interface possess different local atomic environments, and thus nonbonding states can emerge close to the Fermi level; such states significantly reduce the spin polarization at the interface [85,86]; and (ii) charge transfer across the tunnel junction due to the work function difference of the electrodes (see Table I). Since MnVTiAl exhibits the lower work function, electrons flow from the majority-spin (minority-spin) channel of MnVTiAl to the majority-spin (minority-spin) channel of FeVTaAl for parallel (antiparallel) alignment of the magnetization directions of the electrodes. When this charge redistribution reaches equilibrium, MnVTiAl is positively charged near the interface region, whereas FeVTaAl is negatively charged and, as a result, an electric dipole is induced, which affects the electronic as well as the magnetic properties of both electrode materials around the interface region. The loss of HMM and SGS properties at the interface region can be seen in the device density of states (DDOS) presented in Fig. 5 (see also Fig. 2 in the Supplemental Material [87]).

TABLE I.   Material compositions of the considered MTJs, lattice constants a_0, c/a ratio, sublattice and total magnetic moments, work function (Φ), Curie temperatures T_C of the cubic phase, and the electronic ground state. All T_C values are taken from Ref. [61].

SGS/MgO/HMM junction	MgO interface	Compound	a_0 (Å)	c/a	m_X (μ_B)	$m_{X'}$ (μ_B)	m_Y (μ_B)	m_{total} (μ_B)	Φ (eV)	T_C (K)	Ground state
FeVTaAl/MgO/MnVTiAl	FeV-MnV	FeVTaAl	6.10	1.00	0.85	2.38	−0.19	3.00	3.75	681	SGS
		MgO	6.10	0.98					4.53		I
		MnVTiAl	6.10	1.01	−2.42	2.61	0.86	1.00	3.59	963	HMM
FeVTiSi/MgO/CoFeVSb	FeV-CoFe	FeVTiSi	5.91	1.00	0.57	2.33	0.10	3.00	3.52	464	SGS
		MgO	5.91	1.04					4.55		I
		CoFeVSb	5.91	1.12	1.08	1.20	0.78	3.00	4.10	308	HMM

The *I-V* characteristics of the MTJs under consideration are calculated by using two different approaches: (i) the finite-bias NEGF method and (ii) a linear response approach. The latter is computationally much cheaper, while, however, significant differences may appear in the calculated *I-V* curves when compared to the self-consistent NEGF calculations, as will be discussed below. In the middle panels of Figs. 5(a) and 5(b), we present the calculated transmission spectra for the FeVTaAl/MgO/MnVTiAl MTJ for applied bias voltages of +0.3 and −0.3 V for the parallel and antiparallel configurations of the magnetization direction of the electrodes, respectively. The transmission spectrum and consequently the *I-V* curves of the FeVTaAl/MgO/MnVTiAl MTJ displayed in Fig. 6 can be explained on the basis of the DDOS [Figs. 5(a) and 5(b)]. For parallel orientation of the magnetization directions of the electrodes, under forward bias ($V = +0.3$ V), the transmission coefficient for majority-spin electrons is zero due to the gap in the type-II SGS material above the Fermi level. Since MnVTiAl exhibits a gap in the minority-spin channel around the Fermi energy, the transmission coefficient is also zero for minority-spin electrons and thus the MTJ is in the off state, i.e., no current flows through it under forward bias. Under reverse bias ($V = −0.3$ V), majority-spin electrons of occupied states in the SGS electrode FeVTaAl can tunnel into unoccupied states of the HMM electrode MnVTiAl through the MgO tunneling barrier and, as a consequence, the transmission coefficient takes a finite value. In the minority-spin channel, FeVTaAl possesses a gap below E_F and MnVTiAl below and above the Fermi level, and hence, in both materials, no states are available that could contribute to a current within the applied voltage window. Thus, the on current of the MTJ in the parallel configuration is 100% spin polarized.

Switching the magnetization direction of the electrodes from the parallel to the antiparallel configuration results in switching the *I-V* characteristics of the MTJ [see Figs. 1(b) and 1(c)], i.e, the MTJ is in the on state under forward bias, while it is in the off state under reverse bias. In this case, the HMM electrode MnVTiAl possesses a gap in the majority-spin channel and thus this channel does not contribute to the current. However, in the minority-spin channel,

electrons from the occupied states above the Fermi energy in MnVTiAl can tunnel through the MgO tunnel barrier into unoccupied states in FeVTaAl, and thus the transmission coefficient takes a finite value under forward bias, which again leads to a 100% spin polarization of the current. For a reverse bias, no current flows through the MTJ since in the majority-spin channel the HMM electrode MnVTiAl possesses a gap around the Fermi energy, while in the minority-spin channel the SGS electrode FeVTaAl presents a gap below E_F, and hence, for both spin channels, the transmission coefficient is zero.

In Figs. 6(a) and 6(b), we present the *I-V* characteristics of both MTJs within the finite-bias NEGF method, which will be called the self-consistent field (SCF) and the linear response approach (LR) for a MgO thickness of five monolayers (1.1 nm). As seen for the parallel orientation of the magnetization direction of the electrodes, both MTJs are in the off state under forward bias and in the on state under reverse bias. However, this might be seen as contradicting to the conventional *p-n* diodes, in which the diode is in the on state under forward bias. In our case this is a matter of the construction of the MTJ, i.e., by exchanging the electrode materials, one obtains the *I-V* characteristics of conventional diodes. In the SCF calculations, we obtain a monotonic increase of the current *I* with bias voltage *V* for both MTJs with zero turn-on voltages V_T for both FeVTaAl/MgO/MnVTiAl and FeVTiSi/MgO/CoFeVSb junctions in the parallel configuration, respectively. Switching the magnetization direction of the HMM electrode from parallel to antiparallel results in switching the *I-V* characteristics of the MTJs, as shown in Fig. 6(b). Both MTJs are now in the on state under forward bias, while they are in the off state under reverse bias. In contrast to the parallel alignment of the magnetization directions, in this case, the turn-on voltage V_T for the FeVTiSi/MgO/CoFeVSb junction is large, i.e., 0.25 V, which can be understood on the basis of the DDOS presented in the Supplemental Material [87]. The large work function difference of the electrode materials (FeVTiSi and CoFeVSb) gives rise to a band bending in the energy-band diagram of this MTJ and, as a consequence, one obtains an effectively thick tunnel barrier for small bias
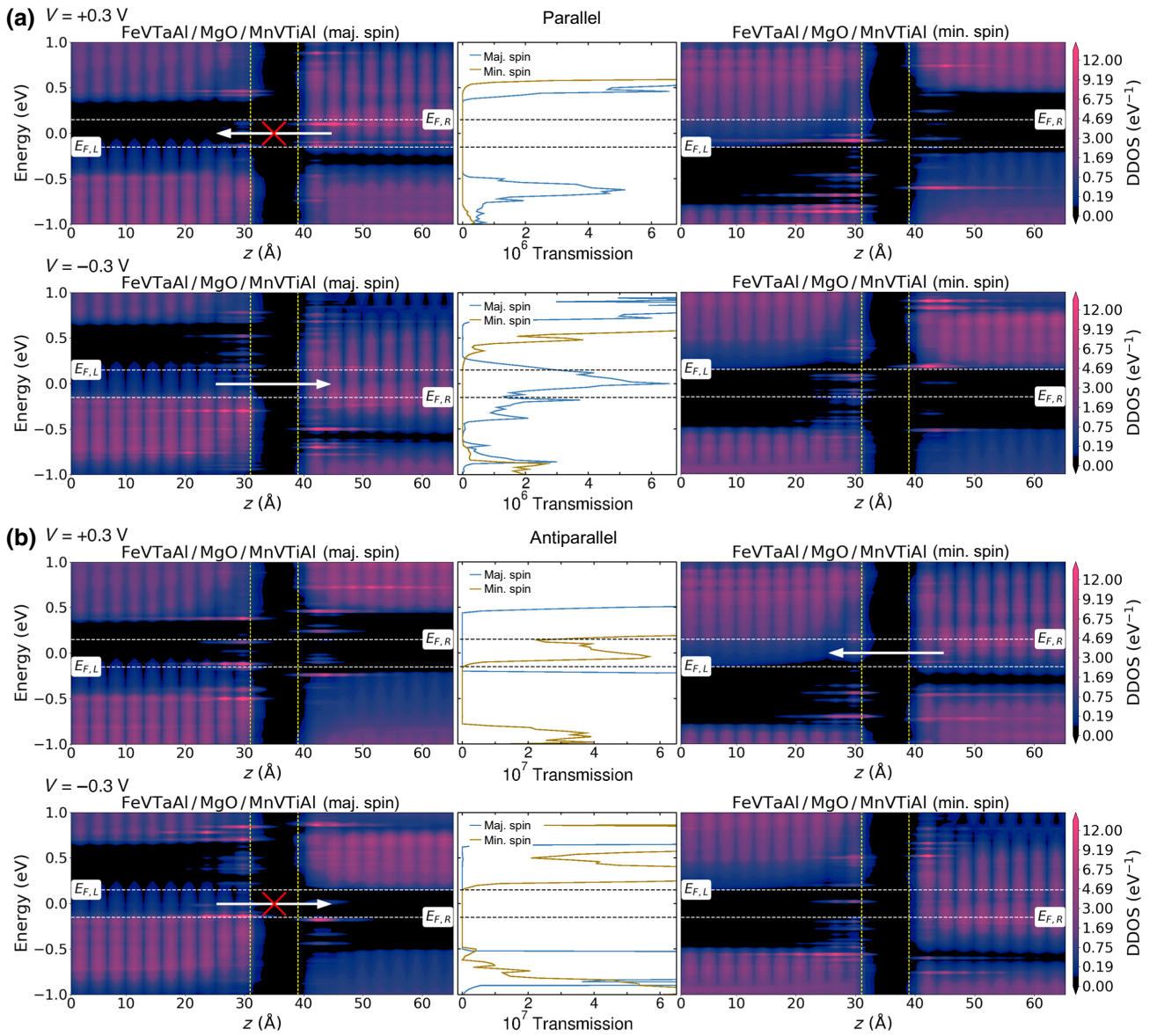
FIG. 5. (a) Projected device density of states (DDOS) for the majority- (left panels) and minority- (right panels) spin channel of the FeVTaAl/MgO/MnVTiAl junction for parallel orientation of the magnetization directions of the electrodes under applied biases of +0.3 and −0.3 V [the corresponding atomic structure is presented in Fig. 4(a)]. In the middle panels we show the calculated transmission spectra for both spin channels. The dashed lines display the Fermi level of the left and right electrodes, while the vertical yellow dashed lines denote the interfaces between the electrodes and MgO. The MgO tunnel barrier thickness is taken to be 1.1 nm, i.e., five monolayers. (b) The same as (a) for antiparallel orientation of the magnetization directions of the electrodes. The majority- and minority-spin channels are illustrated with respect to the magnetic orientation of the left electrode.

voltages, which leads to a large turn-on voltage under forward bias. Furthermore, the on-state currents for parallel and antiparallel configurations of the same MTJ is also quite different. For instance, in the FeVTaAl/MgO/MnVTiAl junction for the parallel configuration the on-state current is one order of magnitude larger than the corresponding current in the antiparallel configuration, while in the FeVTiSi/MgO/CoFeVSb junction the situation is different; here the on-state current is a factor of 2 smaller in the parallel configuration. For

comparison, the *I*-*V* curves obtained from the linear-response approach have been included in Figs. 6(a) and 6(b). As seen, qualitatively the linear response current follows the SCF results with some differences such as the turn-on voltage in the case of the FeVTaAl/Mgo/MnVTiAl junction in the parallel configuration and the overestimated leakage current in the case of the FeVTiSi/MgO/CoFeVSb junction also for the parallel configuration. We do not expect quantitative agreement between these approaches because, for the linear response method, one assumes
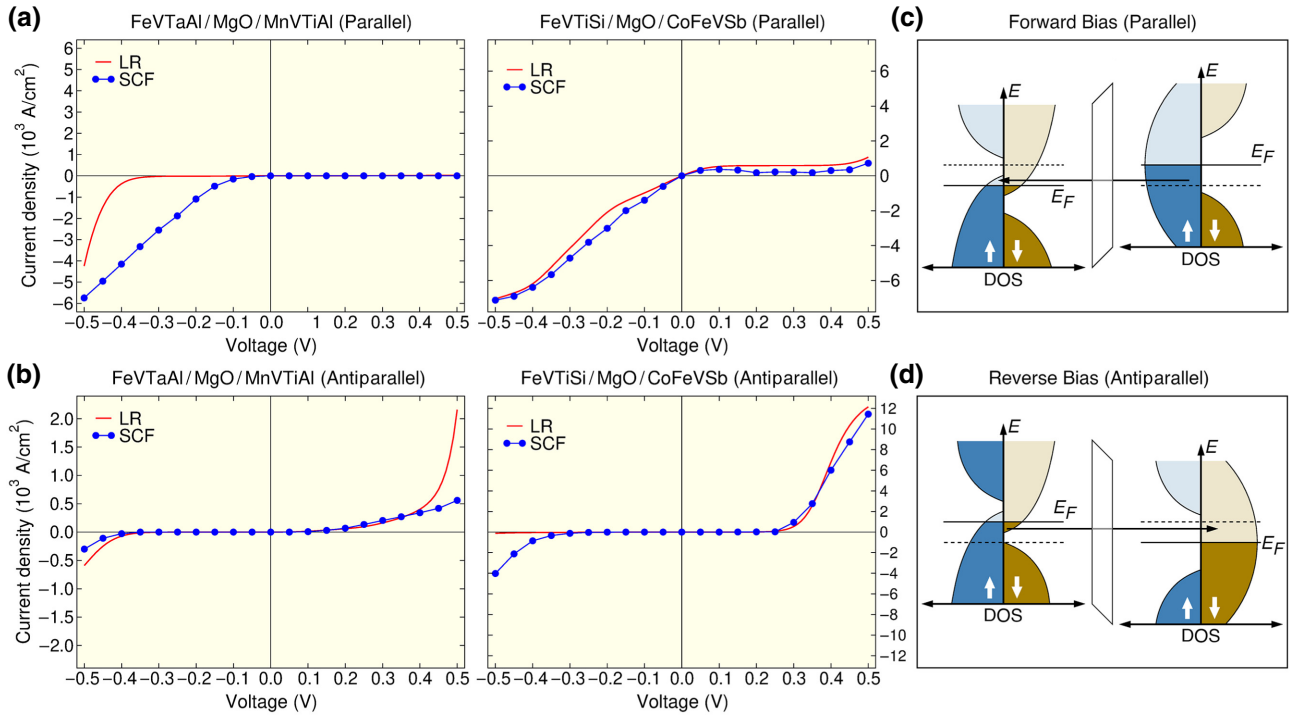
FIG. 6. (a) The current-voltage characteristics for the FeVTaAl/MgO/MnVTiAl (left panel) and FeVTiSi/MgO/CoFeVSb (right panel) junctions for five monolayers of MgO barrier thickness in the parallel configuration. The *I-V* curves are calculated using both SCF and LR methods. (b) The same as (a) for the antiparallel alignment of the magnetization directions of the electrodes. Panels (c) and (d) illustrate the origin of the leakage current under forward and reverse biases for parallel and antiparallel orientations of the magnetization direction of the electrodes, respectively.

a bias-independent transmission spectrum and thus this method is not capable of an accurate description of the *I-V* characteristics. The zero-bias transmission spectrum for the linear response calculations and a discussion of the charge accumulation at the interfaces as well as a detailed analysis of the symmetry character of the band structure of the electrode materials of both MTJs can be found in the Supplemental Material [87].

We would now like to comment on the off-state leakage currents of both MTJs. In principle, at zero temperature, one would obtain a zero off-state current for a perfect SGS electrode. However, in our MTJs both SGS electrodes, FeVTaAl and FeVTiSi, possess a sizeable band overlap between the valence and conduction bands of opposite spin channels around E_F, as schematically illustrated in Figs. 6(c) and 6(d) (see also the supplemental material of Ref. [61] for the DOS). For parallel (antiparallel) aligned magnetization directions of the electrodes, band overlaps allow majority-spin (minority-spin) electrons to tunnel from the occupied states of the HMM (type-II SGS) electrode through the insulating region into unoccupied states of the type-II SGS (HMM) material. Since FeVTiSi possesses an overlap of 150 meV whereas the overlap in FeVTaAl amounts to just 60 meV, a larger leakage current arises in the FeVTiSi/MgO/CoFeVSb junction. At

zero temperature, the obtained on:off current ratios of both MTJs at ± 0.3 V vary between 10^2 and 10^7.

In contrast to conventional semiconductor diodes (*p-n* diode, Schottky diode, Zener diode), in which the rectification bias voltage window (or reverse bias breakdown voltage of the diode) varies between 3–200 V, in the present MTJs, this voltage window is limited by the spin gap of the HMM and SGS Heusler compounds. In analogy to conventional semiconductor diodes, we can express the breakdown voltage for the parallel and antiparallel configurations as $V_B^P = \min\{(SG_{SGS}, E_F^A), (SG_{HMM}, E_F^B)\}$ and $V_B^{AP} = \min\{(SG_{SGS}, E_F^B), (SG_{HMM}, E_F^A)\}$, where (SG_{SGS}, E_F^A) and (SG_{HMM}, E_F^B) stand for the spin gaps of the SGS and HMM electrodes above and below the Fermi energy, respectively. Using the spin gap values of the SGSs and HMMs from Ref. [61], one gets breakdown voltages V_B^P (V_B^{AP}) of 0.31 and -0.34 V (0.33 and -0.30 V) for the parallel (antiparallel) configurations of the FeVTaAl/MgO/MnVTiAl and FeVTiSi/MgO/CoFeVSb MTJs, respectively. Since the estimation of the breakdown voltage is based on the DOS picture of the materials, the calculated V_B^P (V_B^{AP}) values can differ substantially since, as mentioned before, in tunneling processes the bands along the transport direction, their symmetry character, and their matching across the interface play a decisive role. Indeed, the actual calculated

V_B^p values in Fig. 6 are larger than the simple estimated ones for the parallel configuration, while for the antiparallel configuration, the calculated V_B^{AP} values are more close to the estimated ones. However, the simple estimated values set the lower limit of the breakdown voltages V_B^p and V_B^{AP}.

Recently, Maji and Nath reported the fabrication of a MTJ based on Heusler compounds as electrode materials. The junction is composed of HMM Co$_2$MnSi, SGS Ti$_2$CoSi, and a 3-nm MgO tunnel barrier [56]. The authors demonstrated a reconfigurable diode effect with a high on:off ratio and a high TMR ratio that decreases with increasing temperature. Moreover, the breakdown voltage of the MTJ under reverse bias was reported to be around -0.5 V, which is basically the spin gap of the Co$_2$MnSi compound. Indeed, this is the first experimental demonstration of the concept that we proposed in 2019 [55]. Note that Maji and Nath [56] used Ti$_2$CoSi as a SGS electrode; however, this material exhibits type-III SGS behavior in a simple DOS picture [64], whereas in tunneling experiments it behaves like a type-II SGS due to the reasons we discussed above. A detailed discussion of the experiments of Maji and Nath is beyond the scope of the present paper since we were aware of this work after the completion of the present paper. However, we are planning to consider the MTJ of Ref. [56] in a separate future study.

The *I-V* characteristics discussed above as well as the TMR ratio, which we discuss below, in our MTJs are calculated for zero temperature. The temperature effects (non-spin-flip thermal excitations; see Fig. 3) are usually included in NEGF transport calculations of semiconductor devices via the Fermi-Dirac distribution function. However, due to the technical limitation of the QuantumATK

package, as discussed in detail in Ref. [91] for spintronic materials, we neglect these thermal excitations in transport calculations. Moreover, besides high-energy non-spin-flip thermal excitations, temperature affects the magnetic structure and electronic structure of the SGSs and HMMs via Stoner excitations and magnons or collective spin waves. In type-II SGSs, electrons around the Fermi energy can be excited via spin flip with a nearly vanishing amount of energy [see Fig. 2(a)]. Such excitations are known as single-particle Stoner excitations and occupy, in our case, the unoccupied minority-spin states above E_F. As a consequence, these electrons contribute to a leakage current in the antiparallel orientation of the magnetization direction of the type-II SGS and HMM electrode. On the other hand, due to the existence of a gap in HMMs, Stoner excitations are not allowed in these materials. Nevertheless, at finite temperatures, electron-magnon interactions might give rise to the appearance of nonquasiparticle states in the spin gap above the Fermi level of HMMs [92]. As a consequence, these states reduce the spin polarization of the HMM material and thus influence its transport properties. Furthermore, defects at the interface might also affect the characteristics of the SGSs and HMMs and contribute to a leakage current and reduce the on:off ratio and TMR effect.

Finally, we discuss the TMR effect in the MTJs under study. As mentioned above, the reconfigurable diode effect gives rise to an inverse TMR effect in this type of MTJ. The voltage dependence of the TMR ratio for both MTJs is presented in Figs. 7(a) and 7(b) for four different MgO tunnel barrier thicknesses. Because of the computational efficiency, we stick here to the linear response approach; however, for five monolayers of MgO tunnel barrier thickness, we compare the obtained results with the SCF method. For negative bias voltages (reverse bias), both MTJs present a
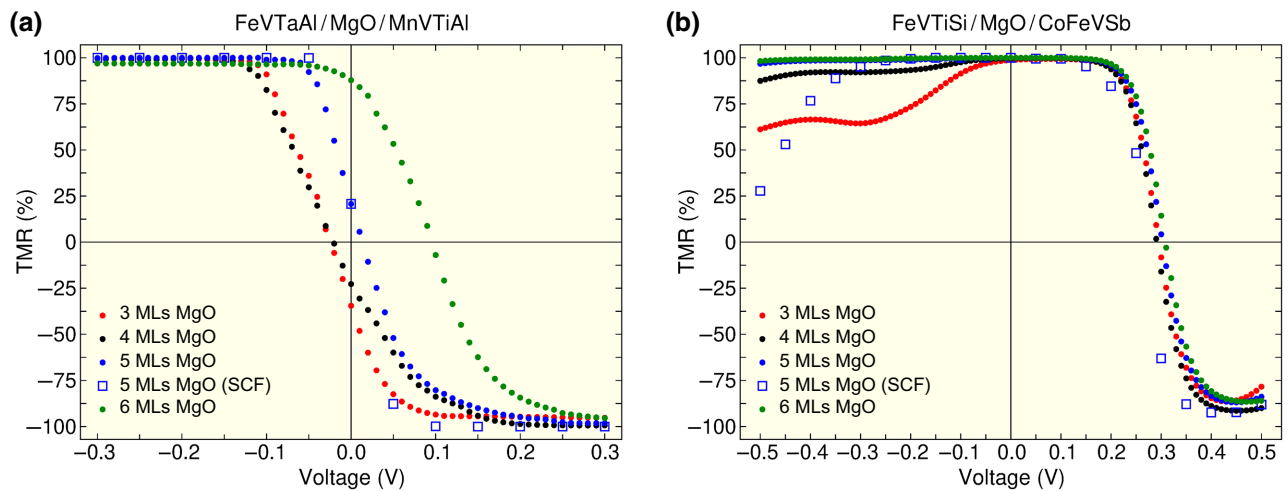

FIG. 7. (a) Voltage dependence of the TMR ratio of the FeVTaAl/MgO/MnVTiAl MTJ for different MgO thicknesses calculated within the linear response approach. For the case of five monolayers (MLs) of MgO thickness, the results are compared with SCF calculations. (b) The same as (a) for the FeVTiSi/MgO/CoFeVSb MTJ.

positive TMR effect, while at a certain applied bias voltage, due to the unique band structure of the SGS electrode, the TMR changes its sign to a negative value, and thus the MTJs exhibits an inverse TMR effect. In principle, for a perfect SGS electrode material, one expects a sharp transition from positive to negative TMR values at zero bias voltage, as displayed in Fig. 1(a); however, in the present MTJs, this transition takes place in a finite voltage window and the transition point is shifted to finite voltages, especially in the FeVTiSi/MgO/CoFeVSb tunnel junction. Two parameters are mainly responsible for the behavior of the TMR curves. These are the on:off current ratio, which reduces the TMR ratio, and the threshold voltage V_T, which causes a voltage shift of the transition point. Like in *I-V* curves, the spin gap of the electrode materials plays an essential role for the TMR ratio and its sign. For instance, in the FeVTiSi/MgO/CoFeVSb tunnel junction the high TMR is obtained in a very small voltage window, especially for negative voltages, and the TMR ratio is significantly reduced for voltages beyond -0.3 V, which is more or less the spin gap of the HMM CoFeVSb material.

V. SUMMARY AND OUTLOOK

MTJs based on Fe, Co, and CoFeB, as well as HMM Heusler compounds, have been extensively studied in spintronics for magnetic memory and magnetic logic applications. Despite their high TMR ratios, especially the MTJs based on HMMs, conventional MTJs do not exhibit current rectification, i.e., a diode effect. A MTJ concept has been proposed in Ref. [55], which exhibits reconfigurable current rectification together with an inverse TMR effect. This MTJ concept was based on HMMs and SGSs and it has recently been demonstrated experimentally using Heusler compounds [56]. In the present work, by employing state-of-the-art DFT and NEGF methods, we design two different MTJs based on the type-II SGS and HMM quaternary Heusler compounds FeVTaAl, FeVTiSi, MnVTiAl, and CoVTiSb. We show that both MTJs [FeVTaAl(001)/MgO/MnVTiAl(001) and FeVTiSi(001)/MgO/CoFeVSb(001)] exhibit a current rectification with a relatively high on:off ratio of up to 10^7. We show that in contrast to conventional semiconductor diodes, such as the *p-n* junction diode or Schottky diode, the rectification bias voltage window (or breakdown voltage) of these MTJs is limited by the spin gap of the HMM and SGS Heusler electrode material, in agreement with recent experiments. A unique feature of the present MTJs is that they can be configured dynamically, i.e., depending on the relative orientation of the magnetization direction of the electrodes, the MTJ allows electrical current to pass either in one or the other direction. This feature gives rise to an inverse TMR effect in such devices. The inverse TMR effect has been investigated as a function of the MgO tunnel barrier thickness. We find that the sign change of the

TMR from a positive to a negative value takes place not at zero bias voltage, but small finite voltages, which can be explained by the on:off ratio (leakage current) and threshold voltage V_T of the MTJs. Moreover, like in *I-V* curves, the spin gap of the electrode materials plays an essential role in the TMR ratio and its sign.

The current nonvolatile magnetic memory technology (STT MRAM and beyond) and several magnetic logic proposals utilize conventional MTJs that have limited functionality. The MTJs based on HMMs and SGSs studied in the present paper provide major advantages over conventional MTJs and open ways to magnetic memory and logic concepts. For instance, these MTJs might be of particular interest for high-density 3D cross-point STT-MRAM applications as they eliminate the need for an additional selection device such as a MOSFET transistor or a *p-n* diode. Apart from memory applications, the MTJs constitute the basic building blocks of the three-terminal magnetic tunnel transistors with unique properties, as discussed in Ref. [55]. Moreover, the present MTJs also open the way to logic-in-memory computing, i.e., storing and processing the data within the same chip and thus providing an opportunity to explore computing architectures beyond the classical von Neumann architecture.

[1] J. von Neumann, First draft of a report on the EDVAC, IEEE Ann. Hist. Comput. **15**, 27 (1993).

[2] M. Horowitz, in *Solid-State Circuits Conference Digest of Technical Papers (ISSCC)* (IEEE International, 2014), p. 10.

[3] H. Li, B. Gao, Z. Chen, Y. Zhao, P. Huang, H. Ye, L. Liu, X. Liu, and J. Kang, A learnable parallel processing architecture towards unity of memory and computing, Sci. Rep. **5**, 13330 (2015).

[4] E. Linn, R. Rosezin, S. Tappertzhofen, U. Böttger, and R. Waser, Beyond von Neumann—logic operations in passive crossbar arrays alongside memory operations, Nanotechnology **23**, 305205 (2012).

[5] T. You, Y. Shuai, W. Luo, N. Du, D. Bürger, I. Skorupa, R. Hübner, S. Henker, C. Mayr, and R. Schüffny, *et al.*, Exploiting memristive BiFeO$_3$ bilayer structures for compact sequential logics, Adv. Funct. Mater. **24**, 3357 (2014).

[6] S. Gao, F. Zeng, M. Wang, G. Wang, C. Song, and F. Pan, Implementation of complete Boolean logic functions in single complementary resistive switch, Sci. Rep. **5**, 15467 (2015).

[7] Y. Zhou, Y. Li, L. Xu, S. Zhong, H. Sun, and X. Miao, 16 Boolean logics in three steps with two anti-serially connected memristors, Appl. Phys. Lett. **106,** 233502 (2015).

[8] Z.-R. Wang, Y.-T. Su, Y. Li, Y.-X. Zhou, T.-J. Chu, K.-C. Chang, T.-C. Chang, T.-M. Tsai, S. M. Sze, and X.-S. Miao, Functionally complete Boolean logic in 1T1R resistive random access memory, IEEE Electron Device Lett. **38,** 179 (2017).

[9] K. M. Kim, N. Xu, X. Shao, K. J. Yoon, H. J. Kim, R. S. Williams, and C. S. Hwang, Single-cell stateful logic using a dual-bit memristor, Phys. Status Solidi Rapid Res. Lett. **13,** 1800629 (2019).

[10] W. Xu, H. Sun, X. Wang, Y. Chen, and T. Zhang, Design of last-level on-chip cache using spin-torque transfer RAM (STT RAM), IEEE Trans. Very Large Scale Integr. (VLSI) Syst. **19,** 483 (2011).

[11] G. Prenat, K. Jabeur, P. Vanhauwaert, G. D. Pendina, F. Oboril, R. Bishnoi, M. Ebrahimi, N. Lamard, O. Boulle, K. Garello, J. Langer, B. Ocker, M.-C. Cyrille, P. Gambardella, M. Tahoori, and G. Gaudin, Ultra-fast and high-reliability SOT-MRAM: From cache replacement to normally-off computing, IEEE Trans. Multi-Scale Comput. Syst. **2,** 49 (2016).

[12] S. Yuasa, T. Nagahama, A. Fukushima, Y. Suzuki, and K. Ando, Giant room-temperature magnetoresistance in single-crystal Fe/MgO/Fe magnetic tunnel junctions, Nat. Mater. **3,** 868 (2004).

[13] S. S. P. Parkin, C. Kaiser, A. Panchula, P. M. Rice, B. Hughes, M. Samant, and S.-H. Yang, Giant tunnelling magnetoresistance at room temperature with MgO (100) tunnel barriers, Nat. Mater. **3,** 862 (2004).

[14] D. Ebke, J. Schmalhorst, N.-N. Liu, A. Thomas, G. Reiss, and A. Hütten, Large tunnel magnetoresistance in tunnel junctions with Co$_2$MnSi/Co$_2$FeSi multilayer electrode, Appl. Phys. Lett. **89,** 162506 (2006).

[15] X. Kou, J. Schmalhorst, A. Thomas, and G. Reiss, Temperature dependence of the resistance of magnetic tunnel junctions with MgO barrier, Appl. Phys. Lett. **88,** 212115 (2006).

[16] G. Reiss, A. Hütten, S. Kämmerer, and J. Schmalhorst, Co$_2$MnSi as full Heusler alloy ferromagnetic electrode in magnetic tunneling junctions, Phys. Status Solidi C **3,** 1322 (2006).

[17] P. Krzysteczko, X. Kou, K. Rott, A. Thomas, and G. Reiss, Current induced resistance change of magnetic tunnel junctions with ultra-thin MgO tunnel barriers, J. Magn. Magn. Mater. **321,** 144 (2009).

[18] J. Mathon and A. Umerski, Theory of tunneling magnetoresistance of an epitaxial Fe/MgO/Fe(001) junction, Phys. Rev. B **63,** 220403(R) (2001).

[19] S. Ikeda, J. Hayakawa, Y. Ashizawa, Y. M. Lee, K. Miura, H. Hasegawa, M. Tsunoda, F. Matsukura, and H. Ohno, Tunnel magnetoresistance of 604% at 300K by suppression of Ta diffusion in CoFeB/MgO/CoFeB pseudo-spin-valves annealed at high temperature, Appl. Phys. Lett. **93,** 082508 (2008).

[20] C. Heiliger, P. Zahn, B. Y. Yavorsky, and I. Mertig, Influence of the interface structure on the bias dependence of tunneling magnetoresistance, Phys. Rev. B **72,** 180406(R) (2005).

[21] C. Heiliger, P. Zahn, B. Y. Yavorsky, and I. Mertig, Interface structure and bias dependence of Fe/MgO/Fe tunnel junctions: *Ab initio* calculations, Phys. Rev. B **73,** 214441 (2006).

[22] S. Jain, A. Ranjan, K. Roy, and A. Raghunathan, Computing in memory with spin-transfer torque magnetic RAM, IEEE Trans. Very Large Scale Integr. (VLSI) Syst. **26,** 470 (2017).

[23] S. K. Kingra, V. Parmar, C.-C. Chang, B. Hudec, T.-H. Hou, and M. Suri, SLIM: Simultaneous logic-in-memory computing exploiting bilayer analog OxRAM devices, Sci. Rep. **10,** 2567 (2020).

[24] R. De Rose, T. Zanotti, F. M. Puglisi, F. Crupi, P. Pavan, and M. Lanuzza, STT-MTJ based smart implication for energy-efficient logic-in-memory computing, Solid State Electron. **184,** 108065 (2021).

[25] R. P. Cowburn and M. E. Welland, Room temperature magnetic quantum cellular automata, Science **287,** 1466 (2000).

[26] I. Amlani, A. O. Orlov, G. Toth, G. H. Bernstein, C. S. Lent, and G. L. Snider, Digital logic gate using quantum-dot cellular automata, Science **284,** 289 (1999).

[27] D. A. Allwood, G. Xiong, C. C. Faulkner, D. Atkinson, D. Petit, and R. P. Cowburn, Magnetic domain-wall logic, Science **309,** 1688 (2005).

[28] M. Tsoi, R. E. Fontana, and S. S. P. Parkin, Magnetic domain wall motion triggered by an electric current, Appl. Phys. Lett. **83,** 2617 (2003).

[29] R. Richter, L. Bär, J. Wecker, and G. Reiss, Nonvolatile field programmable spin-logic for reconfigurable computing, Appl. Phys. Lett. **80,** 1291 (2002).

[30] A. Ney, C. Pampuch, R. Koch, and K. Ploog, Programmable computing with a single magnetoresistive element, Nature **425,** 485 (2003).

[31] A. Thomas, D. Meyners, D. Ebke, N.-N. Liu, M. D. Sacher, J. Schmalhorst, G. Reiss, H. Ebert, and A. Hütten, Inverted spin polarization of Heusler alloys for spintronic devices, Appl. Phys. Lett. **89,** 012502 (2006).

[32] H. Dery, P. Dalal, L. Cywiński, and L. J. Sham, Spin-based logic in semiconductors for reconfigurable large-scale circuits, Nature **447,** 573 (2007).

[33] B. Behin-Aein, D. Datta, S. Salahuddin, and S. Datta, Proposal for an all-spin logic device with built-in memory, Nat. Nanotechnol. **5,** 266 (2010).

[34] J. S. Friedman and A. V. Sahakian, Complementary magnetic tunnel junction logic, IEEE Trans. Electron Devices **61,** 1207 (2014).

[35] S. Isogami and T. Owada, Electronic circuit using magnetic tunnel junctions with normal and inverse magnetoresistive effects, IEEJ Trans. Electr. Electron. Eng. **9,** S73 (2014).

[36] D. M. Bromberg, D. H. Morris, L. Pileggi, and J.-G. Zhu, Novel STT-MTJ device enabling all-metallic logic circuits, IEEE Trans. Magn. **48,** 3215 (2012).

[37] S. Fukami, T. Suzuki, K. Nagahara, N. Ohshima, Y. Ozaki, S. Saito, R. Nebashi, N. Sakimura, H. Honjo, and K. Mori, *et al.*, in *2009 Symposium on VLSI Technology* (IEEE, 2009), p. 230.

[38] W. Kang, C. Zheng, Y. Zhang, D. Ravelosona, W. Lv, and W. Zhao, Complementary spintronic logic with spin Hall

effect-driven magnetic tunnel junction, IEEE Trans. Magn. **51**, 1 (2015).

[39] C. de Buttet, M. Hehn, F. Montaigne, C. Tiusan, G. Malinowski, A. Schuhl, E. Snoeck, and S. Zoll, Low-resistance magnetic tunnel junctions with an $MgO - Al_2O_3$ composite tunnel barrier: Asymmetric transport characteristics and free electron modeling of a self-limited oxidation bilayer, Phys. Rev. B **73**, 104439 (2006).

[40] M. Chshiev, D. Stoeffler, A. Vedyayev, and K. Ounadjela, Magnetic diode effect in double-barrier tunnel junctions, EPL **58**, 257 (2002).

[41] C. Tiusan, M. Chshiev, A. Iovan, V. Da Costa, D. Stoeffler, T. Dimopoulos, and K. Ounadjela, Quantum coherent transport versus diode-like effect in semiconductor-free metal/insulator structure, Appl. Phys. Lett. **79**, 4231 (2001).

[42] A. Iovan, S. Andersson, Y. G. Naidyuk, A. Vedyaev, B. Dieny, and V. Korenivski, Spin diode based on Fe/MgO double tunnel junction, Nano Lett. **8**, 805 (2008).

[43] S. van Dijken, X. Jiang, and S. S. P. Parkin, Spin-dependent hot electron transport in $Ni_{81}Fe_{19}$ and $Co_{84}Fe_{16}$ films on GaAs(001), Phys. Rev. B **66**, 094417 (2002).

[44] R. Sato and K. Mizushima, Spin-valve transistor with an Fe/Au/Fe(001) base, Appl. Phys. Lett. **79**, 1157 (2001).

[45] G. Rodary, M. Hehn, T. Dimopoulos, D. Lacour, J. Bangert, H. Jaffrès, F. Montaigne, F. N. Van Dau, F. Petroff, and A. Schuhl, *et al.*, Development of a magnetic tunnel transistor based on a double tunnel junction, J. Magn. Magn. Mater. **290**, 1097 (2005).

[46] M. Gobbi, A. Bedoya-Pinto, F. Golmar, R. Llopis, F. Casanova, and L. Hueso, C_{60}-based hot-electron magnetic tunnel transistor, Appl. Phys. Lett. **101**, 102404 (2012).

[47] J. H. Lee, K.-I. Jun, K.-H. Shin, S. Y. Park, J. K. Hong, K. Rhie, and B. C. Lee, Large magnetocurrents in double-barrier tunneling transistors, J. Magn. Magn. Mater. **286**, 138 (2005).

[48] T. Nagahama, H. Saito, and S. Yuasa, Hot electron transport in magnetic tunnel transistors with an epitaxial MgO tunnel barrier, Appl. Phys. Lett. **96**, 112509 (2010).

[49] R. Aluguri and T.-Y. Tseng, Notice of violation of IEEE publication principles: Overview of selector devices for 3-D stackable cross point RRAM arrays, IEEE J. Electron Devices Soc. **4**, 294 (2016).

[50] G. W. Burr, R. S. Shenoy, K. Virwani, P. Narayanan, A. Padilla, B. Kurdi, and H. Hwang, Access devices for 3D crosspoint memory, J. Vac. Sci. Technol. B Nanotechnol. Microelectron. **32**, 040802 (2014).

[51] X. Peng, R. Madler, P.-Y. Chen, and S. Yu, Cross-point memory design challenges and survey of selector device characteristics, J. Comput. Electron. **16**, 1167 (2017).

[52] D. E. Nikonov, G. I. Bourianoff, and T. Ghani, Proposal of a spin torque majority gate logic, IEEE Electron Device Lett. **32**, 1128 (2011).

[53] D. E. Nikonov and I. A. Young, Benchmarking of beyond-CMOS exploratory devices for logic integrated circuits, IEEE J. Explor. Solid-State Comput. Devices Circuits **1**, 3 (2015).

[54] C. Pan and A. Naeemi, An expanded benchmarking of beyond-CMOS devices based on Boolean and neuromorphic representative circuits, IEEE J. Explor. Solid-State Comput. Devices Circuits **3**, 101 (2017).

[55] E. Şaşıoğlu, S. Blügel, and I. Mertig, Proposal for reconfigurable magnetic tunnel diode and transistor, ACS Appl. Electron. Mater. **1**, 1552 (2019).

[56] N. Maji and T. K. Nath, Demonstration of reconfigurable magnetic tunnel diode and giant tunnel magnetoresistance in magnetic tunnel junctions made with spin gapless semiconductor and half-metallic Heusler alloy, Appl. Phys. Lett. **120**, 072401 (2022).

[57] X. L. Wang, Proposal for a New Class of Materials: Spin Gapless Semiconductors, Phys. Rev. Lett. **100**, 156404 (2008).

[58] R. A. de Groot, F. M. Mueller, P. G. v. van Engen, and K. H. J. Buschow, New Class of Materials: Half-Metallic Ferromagnets, Phys. Rev. Lett. **50**, 2024 (1983).

[59] K. Özdoğan, E. Şaşıoğlu, and I. Galanakis, Slater-Pauling behavior in LiMgPdSn-type multifunctional quaternary Heusler materials: Half-metallicity, spin-gapless and magnetic semiconductors, J. Appl. Phys. **113**, 193903 (2013).

[60] Q. Gao, I. Opahle, and H. Zhang, High-throughput screening for spin-gapless semiconductors in quaternary Heusler compounds, Phys. Rev. Mater. **3**, 024410 (2019).

[61] T. Aull, E. Şaşıoğlu, I. V. Maznichenko, S. Ostanin, A. Ernst, I. Mertig, and I. Galanakis, *Ab initio* design of quaternary Heusler compounds for reconfigurable magnetic tunnel diodes and transistors, Phys. Rev. Mater. **3**, 124415 (2019).

[62] X. Wang, G. Peleckis, C. Zhang, H. Kimura, and S. Dou, Colossal electroresistance and giant magnetoresistance in doped $PbPdO_2$ thin films, Adv. Mater. **21**, 2196 (2009).

[63] G. Z. Xu, E. K. Liu, Y. Du, G. J. Li, G. D. Liu, W. H. Wang, and G. H. Wu, A new spin gapless semiconductors family: Quaternary Heusler compounds, EPL **102**, 17007 (2013).

[64] S. Skaftouros, K. Özdoğan, E. Şaşıoğlu, and I. Galanakis, Search for spin gapless semiconductors: The case of inverse Heusler compounds, Appl. Phys. Lett. **102**, 022402 (2013).

[65] I. Galanakis, K. Özdoğan, and E. Şaşıoğlu, Spin-filter and spin-gapless semiconductors: The case of Heusler compounds, AIP Adv. **6**, 055606 (2016).

[66] S. Ouardi, G. H. Fecher, C. Felser, and J. Kübler, Realization of Spin Gapless Semiconductors: The Heusler Compound Mn_2CoAl, Phys. Rev. Lett. **110**, 100401 (2013).

[67] J. Bardeen, Tunnelling from a Many-Particle Point of View, Phys. Rev. Lett. **6**, 57 (1961).

[68] R. Meservey and P. M. Tedrow, Spin-polarized electron tunneling, Phys. Rep. **238**, 173 (1994).

[69] M. Julliere, Tunneling between ferromagnetic films, Phys. Lett. A **54**, 225 (1975).

[70] A. M. Bratkovsky, Assisted tunneling in ferromagnetic junctions and half-metallic oxides, Appl. Phys. Lett. **72**, 2334 (1998).

[71] J. Inoue and S. Maekawa, Effects of spin-flip and magnon-inelastic scattering on tunnel magnetoresistance, J. Magn. Magn. Mater. **198**, 167 (1999).

[72] J. Schmalhorst, S. Kämmerer, G. Reiss, and A. Hütten, Inelastic electron tunneling spectroscopy and bias voltage dependence of magnetic tunnel junctions with polycrystalline Co_2MnSi electrode, Appl. Phys. Lett. **86**, 052501 (2005).

[73] S. Smidstrup, D. Stradi, J. Wellendorff, P. A. Khomyakov, U. G. Vej-Hansen, M.-E. Lee, T. Ghosh, E. Jónsson, H.

Jónsson, and K. Stokbro, First-principles Green's-function method for surface calculations: A pseudopotential localized basis set approach, Phys. Rev. B **96,** 195309 (2017).

[74] S. Smidstrup, *et al.*, QuantumATK: An integrated platform of electronic and atomic-scale modelling tools, J. Phys. Condens. Matter **32,** 015901 (2020).

[75] M. J. Van Setten, M. Giantomassi, E. Bousquet, M. J. Verstraete, D. R. Hamann, X. Gonze, and G.-M. Rignanese, The PseudoDojo: Training and grading a 85 element optimized norm-conserving pseudopotential table, Comput. Phys. Commun. **226,** 39 (2018).

[76] J. P. Perdew, K. Burke, and M. Ernzerhof, Generalized Gradient Approximation Made Simple, Phys. Rev. Lett. **77,** 3865 (1996).

[77] J. P. Perdew, S. Kurth, A. Zupan, and P. Blaha, Accurate Density Functional with Correct Formal Properties: A Step Beyond the Generalized Gradient Approximation, Phys. Rev. Lett. **82,** 2544 (1999).

[78] J. P. Perdew, W. Yang, K. Burke, Z. Yang, E. K. U. Gross, M. Scheffler, G. E. Scuseria, T. M. Henderson, I. Y. Zhang, A. Ruzsinszky, H. Peng, J. Sun, E. Trushin, and A. Görling, Understanding band gaps of solids in generalized Kohn–Sham theory, Proc. Natl. Acad. Sci. **114,** 2801 (2017).

[79] P. Borlido, T. Aull, A. W. Huran, F. Tran, M. A. Marques, and S. Botti, Large-scale benchmark of exchange–correlation functionals for the determination of electronic band gaps of solids, J. Chem. Theory Comput. **15,** 5069 (2019).

[80] L. G. Ferreira, M. Marques, and L. K. Teles, Approximation to density functional theory for the calculation of band gaps of semiconductors, Phys. Rev. B **78,** 125116 (2008).

[81] L. G. Ferreira, M. Marques, and L. K. Teles, Slater half-occupation technique revisited: The LDA-1/2 and GGA-1/2 approaches for atomic ionization energies and band gaps in semiconductors, AIP Adv. **1,** 032119 (2011).

[82] M. Büttiker, Y. Imry, R. Landauer, and S. Pinhas, Generalized many-channel conductance formula with application to small rings, Phys. Rev. B **31,** 6207 (1985).

[83] W. H. Butler, X.-G. Zhang, T. C. Schulthess, and J. M. MacLaren, Spin-dependent tunneling conductance of Fe|MgO|Fe sandwiches, Phys. Rev. B **63,** 054416 (2001).

[84] S. V. Faleev, Y. Ferrante, J. Jeong, M. G. Samant, B. Jones, and S. S. P. Parkin, Heusler compounds with perpendicular

magnetic anisotropy and large tunneling magnetoresistance, Phys. Rev. Mater. **1,** 024402 (2017).

[85] Y. Miura, H. Uchida, Y. Oba, K. Nagao, and M. Shirai, Coherent tunnelling conductance in magnetic tunnel junctions of half-metallic full Heusler alloys with MgO barriers, J. Phys.: Condens. Matter **19,** 365228 (2007).

[86] Y. Miura, H. Uchida, Y. Oba, K. Abe, and M. Shirai, Half-metallic interface and coherent tunneling in $Co_2 YZ/MgO/Co_2 YZ$ ($YZ = MnSi, CrAl$) magnetic tunnel junctions: A first-principles study, Phys. Rev. B **78,** 064416 (2008).

[87] See Supplemental Material at http://link.aps.org/supplemental/10.1103/PhysRevApplied.18.034024 for a table listing the spin gap values below and above the Fermi level for the spin-gapless and half-metallic Heusler compounds, the zero-bias transmission spectrum for both MTJs (FeVTaAl/MgO/MnVTiAl and FeVTiSi/MgO/CoFeVSb), the DDOS, the transmission spectrum of the FeVTiSi/MgO/CoFeVSb junction in the antiparallel configuration at equilibrium (zero bias) as well as for an applied bias voltage of $+0.2$ V, a detailed symmetry analysis of the band character of both magnetic tunnel junctions, and a discussion of the charge accumulation in the FeVTaAl/MgO/MnVTiAl junction. References [88–90] are included in the Supplemental Material.

[88] L. P. Bouckaert, R. Smoluchowski, and E. Wigner, Theory of Brillouin zones and symmetry properties of wave functions in crystals, Phys. Rev. **50,** 58 (1936).

[89] K. D. Belashchenko, E. Y. Tsymbal, M. van Schilfgaarde, D. A. Stewart, I. I. Oleynik, and S. S. Jaswal, Effect of interface bonding on spin-dependent tunneling from the oxidized Co surface, Phys. Rev. B **69,** 174408 (2004).

[90] N. F. Hinsche, M. Fechner, P. Bose, S. Ostanin, J. Henk, I. Mertig, and P. Zahn, Strong influence of complex band structure on tunneling electroresistance: A combined model and *ab initio* study, Phys. Rev. B **82,** 214110 (2010).

[91] E. Şaşıoğlu, T. Aull, D. Kutschabsky, S. Blügel, and I. Mertig, Half-Metal–Spin-Gapless-Semiconductor Junctions as a Route to the Ideal Diode, Phys. Rev. Appl. **14,** 014082 (2020).

[92] M. I. Katsnelson, V. Y. Irkhin, L. Chioncel, A. I. Lichtenstein, and R. A. de Groot, Half-metallic ferromagnets: From band structure to many-body effects, Rev. Mod. Phys. **80,** 315 (2008).